PERGAMON

Journal of Structural Geology 24 (2002) 45–55

JOURNAL OF STRUCTURAL GEOLOGY

www.elsevier.com/locate/jstrugeo

Sheath folds formed by drag induced by rotation of rigid inclusions in viscous simple shear flow: nature and experiment

F. Rosas*, F.O. Marques, A. Luz, S. Coelho

LATTEX, Fac. Ciências, Univ. Lisboa, Edifício C2, Piso 5, 1749-016 Lisboa, Portugal

Received 14 August 2000; revised 12 March 2001; accepted 26 March 2001

Abstract

Natural examples of fold patterns associated with rotated boudins occur in the Ossa–Morena Zone (S Portugal) and triggered the present study. In ductile marbles with embedded competent mafic boudins, the folds seem to have originated by rotation of these bodies and show differential development, from gentle deflections to sheath folds. This suggests a dependence of the structure type on the distance of the metamorphic layering to the rigid body. The experimental work presented here was performed with rotating inclusions in bulk simple shear and introduces a new variable, the distance of the marker layer from the rigid inclusion (d), expressed in terms of E, the ratio between the spacing between marker layers (D) and the greater principal dimension of the inclusion (a). Contrary to previous experimental work in the literature, we used planar marker layers without concomitant boudinage. Our results show new processes of development of sheath folds from planar layers, and also that some non-cylindrical layer deflections are transient and, thus, that sheath folds do not originate from them. When d is small and the inclusion starts with its longest axis normal to the shear plane, sheath folds develop by drag pull processes on originally planar marker layers. Transient non-cylindrical deflections develop on originally planar marker layers when the distance between the marker layers is smaller than the longest principal dimension of the rigid particle.

The monoclinic symmetry of the drag sheath fold patterns associated with rotating rigid inclusions indicate non-coaxial flow and can be used as a shear sense criterion (quarter structure).

Keywords: Fold patterns; Rotated boudins; Drag push and pull; Analogue modelling

1. Introduction

The development of sheath folds around rigid inclusions in bulk simple shear has been the subject of investigation in recent years. Cobbold and Quinquis (1980) showed that sheath folds can develop associated with boudinage in bulk simple shear (their Model 3) or from passive non-cylindrical deflections on foliations (their Model 1). Marques and Cobbold (1995) discussed sheath fold development associated with competent inclusions (boudins) which, as in Cobbold and Quinquis (1980), show little or no rotation with respect to the shear plane (reference frame composed of orthogonal axes X, Y and Z, with the shear plane parallel to the XY plane, and X coincident with the shear direction). Conversely, Rosas et al. (2001) worked with rotating inclusions in simple shear to study different sheath fold development as a function of the amount and angular velocity of rotation of associated rigid inclusions. They concluded that well-developed sheath folds are expected to form around little rotated rigid bodies, whereas only minor (or none) sheath folds would occur around rotating inclusions.

Rosas et al. (2001) studied the development of sheath folds as a function of just aspect ratio and original orientation of the competent inclusions. The present experimental work was also performed with rotating inclusions in bulk simple shear, but introduces a new variable: the distance of the marker layer from the rigid inclusion (d). The rigid inclusion acts as an obstacle and disturbs laminar flow, and because this effect increases towards the inclusion, we studied the influence of d on sheath fold development. The distance effect was tested with initial planar marker layers, or with initially deflected marker layers as in Cobbold and Quinquis (1980) and Marques and Cobbold (1995).

2. Natural example

Our experiments were based on field observations carried out along a geotraverse in the western Ossa–Morena Zone, Southern Iberian Variscan Fold Belt, southern Portugal. It

* Corresponding author.
E-mail address: frosas@fc.ul.pt (F. Rosas).

0191-8141/02/$ - see front matter
PII: S0191-8141(01)00046-3

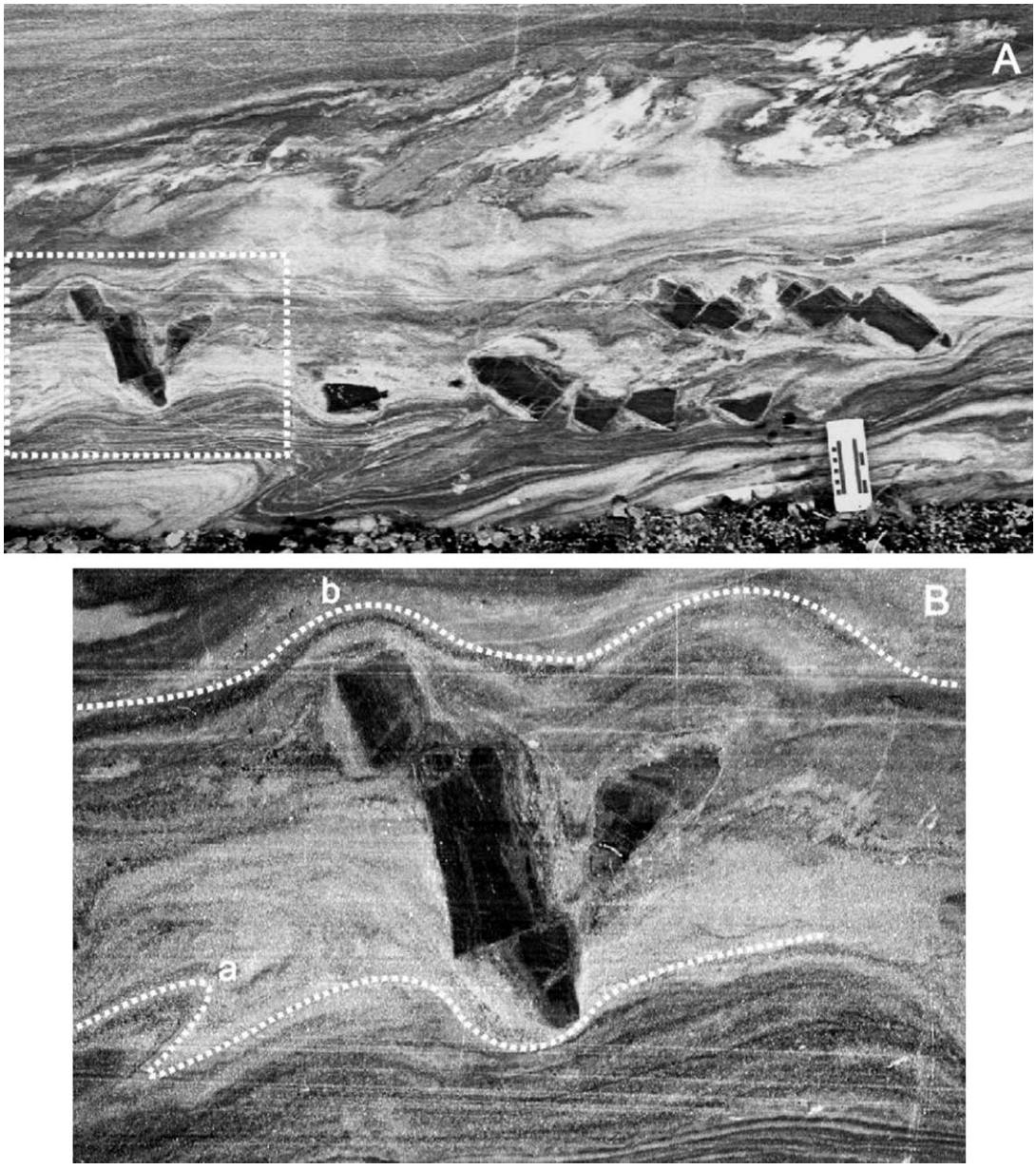

Fig. 1. (A) General view of the studied outcrop. (B) Close up of the contoured area in (A). Note the fold pattern in a and b, and similarity with experimental pattern in Fig. 6.

includes a unit of marbles, with embedded amphibolite boudins, affected by a pervasive mylonitic foliation and by a N–S trending mineral stretching lineation. The rheological contrast between incompetent marbles and competent boudins resulted in deflections of the foliation. In some cases (Fig. 1A), later shearing transformed these deflections into well-developed sheath folds (Fig. 2) associated with boudins of parallelepiped shape parallel to the mylonitic foliation. These boudins are interpreted to have remained practically non-rotated relative to the shear plane during progressive deformation (Rosas et al., 2001) and, thus, the fold patterns developed according to the results of Cobbold and Quinquis (1980, Model 3) and Marques and Cobbold (1995). In other cases (Fig. 1B), the boudin is interpreted to have rotated significantly and a particular structural pattern developed that includes sheath folds. The study of these structures triggered our experimental work.

3. Experimental procedure

Our experiments were performed in bulk simple shear because the natural example (Fig. 1A) is interpreted to have formed in a non-coaxial deformation regime, mainly bulk layer-parallel simple shear, with a subordinate component of layer-normal pure shear. The existence of a significant layer-normal component of flattening would inhibit rotations like the one deduced for the boudin in Fig. 1B,

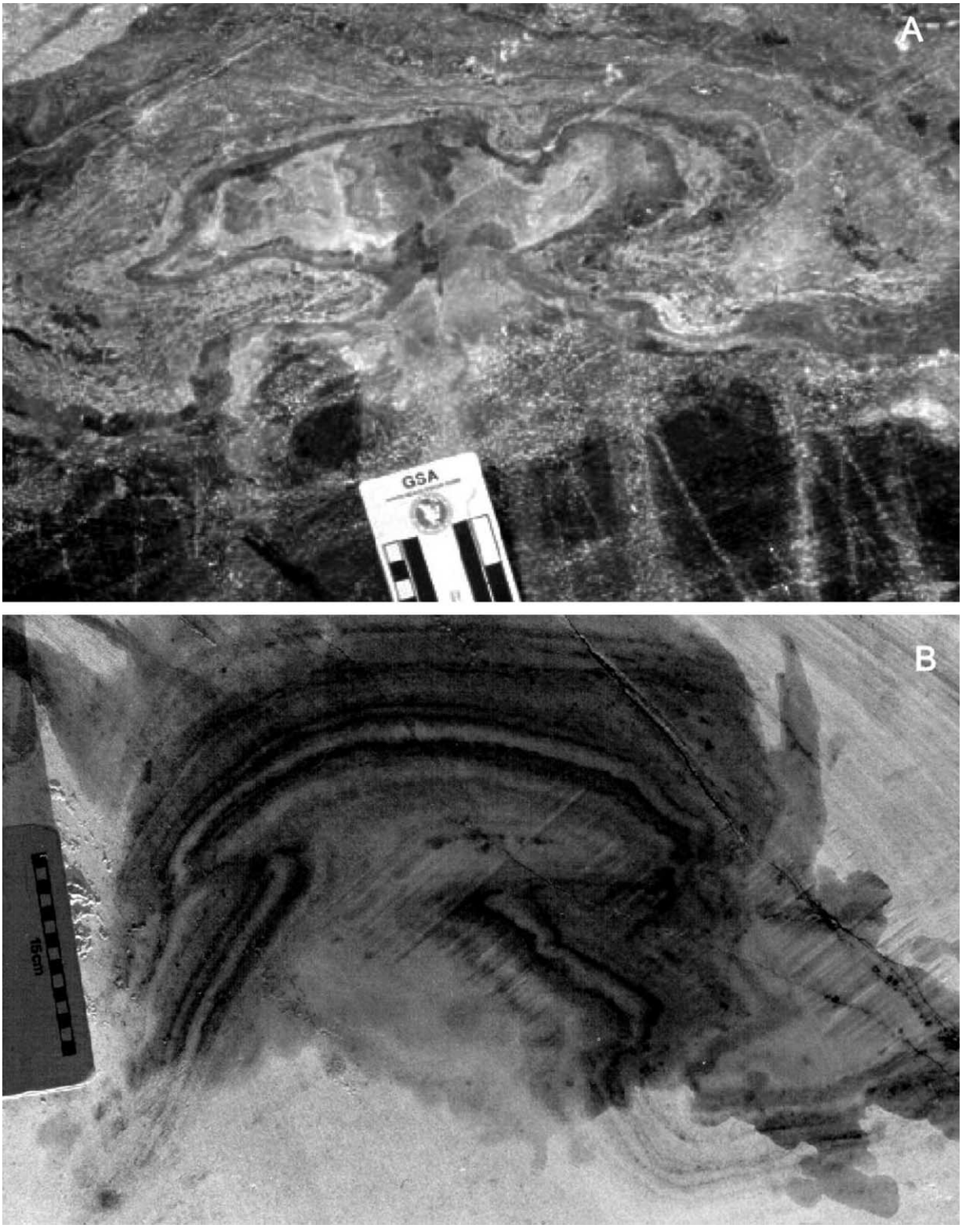

Fig. 2. Cross-sections of sheath folds with mushroom aspect in the studied marbles.

and the boudin would have stabilised at a low angle to the shear plane (Ghosh and Ramberg, 1976).

As discussed in Rosas et al. (2001), from recent literature (Talbot 1999; Treagus 1999) no methods seem to be suitable to obtain accurate determination of the viscosity contrast between marble (incompetent matrix) and amphibolite (competent boudins). Nevertheless, from direct field observation of the different types of structures that formed in each

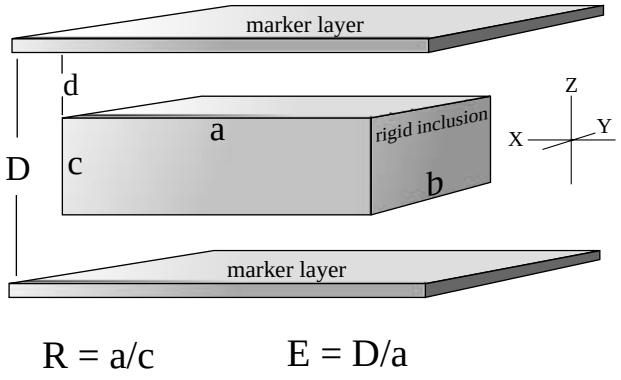

Fig. 3. Initial stage, geometry, variables and kinematic axes.

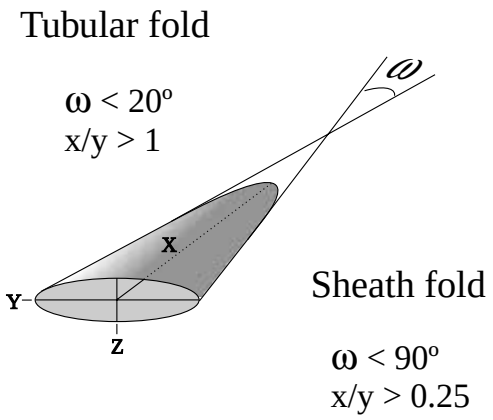

Fig. 4. Definitions of sheath and tubular folds according to Skjernaa (1989).

one of those lithologies, it is possible to conclude that such a contrast is large: in the marbles the metamorphic layering is strongly folded, whereas in the amphibolites structures are simply represented by fractured boudins.

In our experiments, we used the same analogue materials employed by other authors that modelled structures resulting from high viscosity contrasts in rocks (e.g. Ramberg 1959; Ghosh and Ramberg, 1976; Van Den Driessche and Brun 1987; Marques and Cobbold 1995; Rosas et al., 2001): transparent silicone putty to simulate the incompetent marble matrix (polydimethyl–siloxane — a PDMS manufactured by Dow Corning of Great Britain under the trade name SGM 36 — for physical properties and convenience as geological model materials; see Weijermars, 1986); pink silicone putty as a passive strain marker (Rhodorsil gomme speciale 70009 manufactured by Rhone–Poulenc, France; viscosity contrast between SGM36 and RGS70009 is not significant; Weijermars, 1986) and a rigid plastic as an analogue for the competent mafic boudins.

Table 1
Summary of experimental results. $E = D/a$

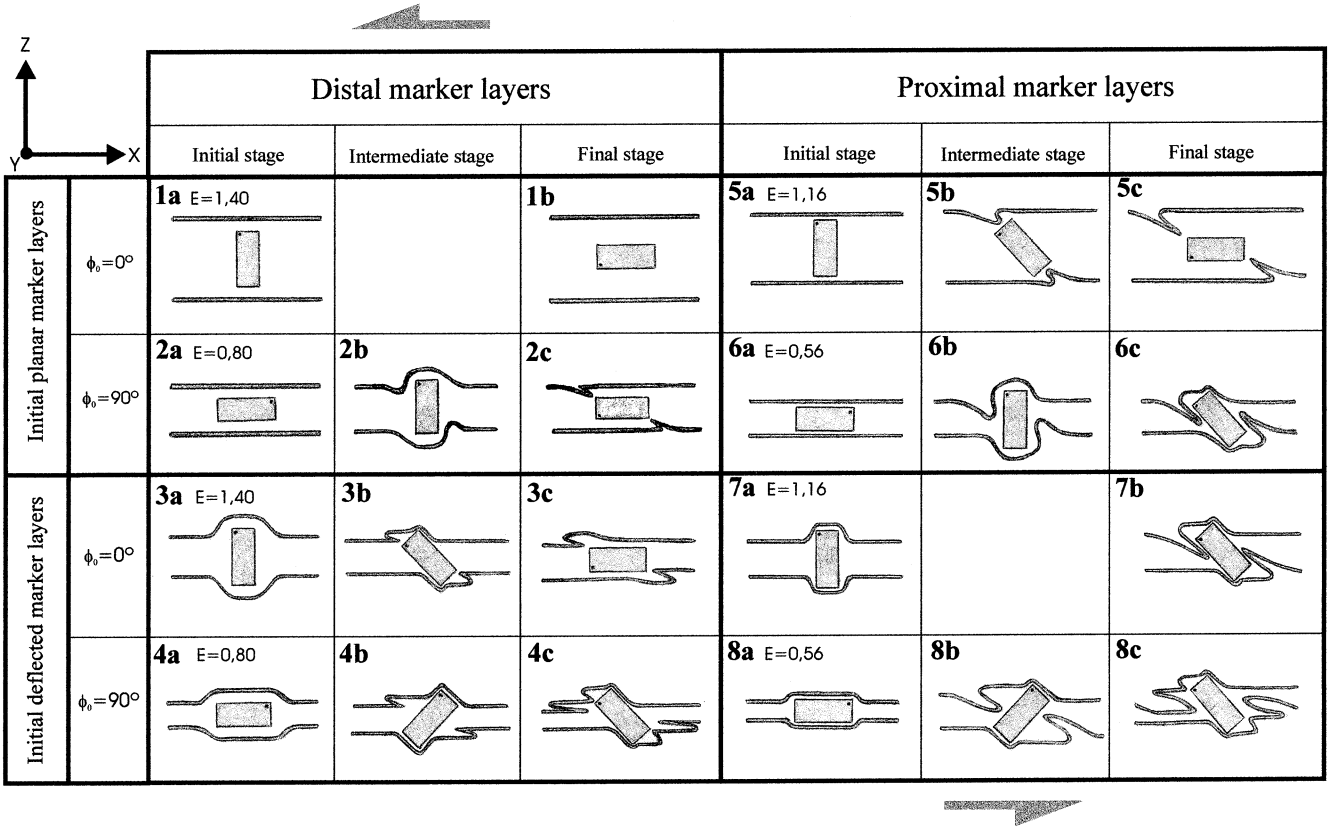

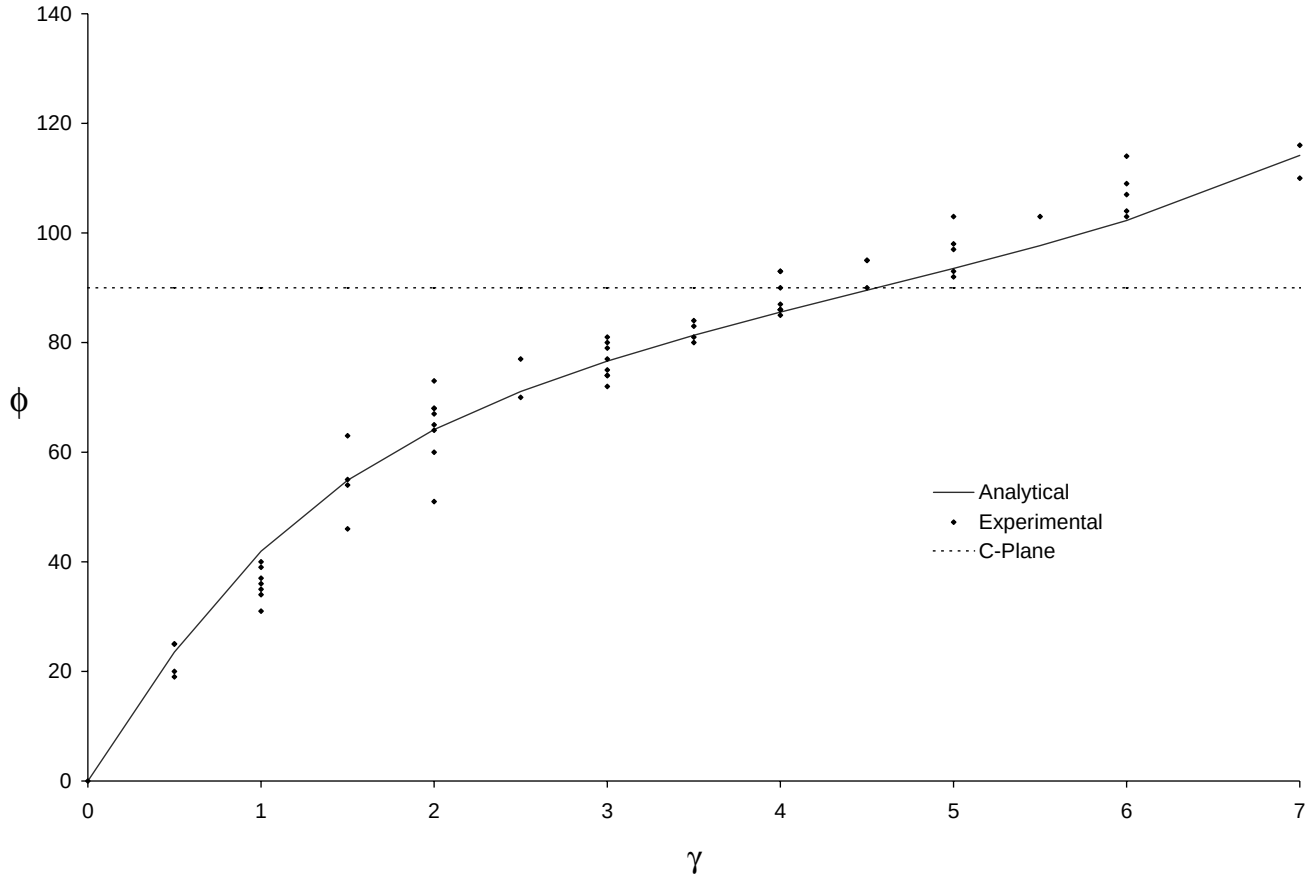

Fig. 5. Graph with measured ϕ at regular intervals in several experiments and comparison with analytical curve from Ghosh and Ramberg (1976). ϕ is the angle between *Z* (axis normal to the shear plane) and *a* (greater principal dimension of the inclusion), γ is the shear strain and *C-plane* is the shear plane and corresponds to the XY plane.

Our experiments were carried out in the same simple shear rig used by Rosas et al. (2001). The co-ordinate system used was *X, Y* and *Z* for the matrix: the shear plane was coincident with the *XY* plane and *X* was the shear direction. The inclusions were of parallelepiped shape with dimensions defined as *a, b* and *c* ($25 \times 12 \times 10$ mm^3) (Fig. 3). *a/c* was the axial ratio of the inclusion (*R*). Perfect adherence of the PDMS to the *XY* walls ensured that shear was integrally transmitted to the model, whereas a neutral liquid soap was used to guarantee that friction was minimum on all other walls to avoid boundary effects.

In all experiments the rig was filled with PDMS with a rigid inclusion immersed in the middle. Two marker layers (2 mm thick) were placed inside the transparent silicone putty, parallel to the *XY* plane, to represent passive markers at a distance *D* from each other (Fig. 3 and Table 1 — initial stage of the models). These marker layers and the inclusion were always separated by a layer of PDMS of variable thickness — defining *d*, the marker layer distance from the rigid inclusion (Fig. 3). *E* is defined as the ratio between *D* and *a* ($E = D/a$).

The initial orientation of the inclusions (ϕ_0 — angle between *a* and *Z*) was, following Ghosh and Ramberg's (1976) notation (Table 1): (1) *a* parallel to *X* ($\phi_0 = 90°$) and *b* coincident with *Y*, and (2) *a* parallel to *Z* ($\phi_0 = 0°$) and *b* also coincident with *Y*.

In this work we followed the definitions of sheath and tubular folds proposed by Skjernaa (1989): non-cylindrical folds with $\omega < 90°$ and $x{:}y > 1/4$, and $\omega < 20°$ and $x{:}y > 1$, respectively (ω, *x*, *y* as defined in Fig. 4). In our experiments, the values of ω depended on shear strain (γ), on *b* and on degree of rotation of the rigid inclusion (ϕ), because *x* depended on γ and *y* was approximately equal to *b*. Thus, the earlier folds had curved hinges and were not true sheath folds as defined above, but gradually evolved into true sheath to tubular folds with increasing γ.

We measured ϕ at regular intervals in several experiments and the results are shown in the graph of Fig. 5. The graph illustrates that our results are very similar to the theoretical predictions of Ghosh and Ramberg (1976), which is important to show that the shear zone thickness did not interfere with the rotation of the inclusion. It also shows that flow was close to viscous simple shear.

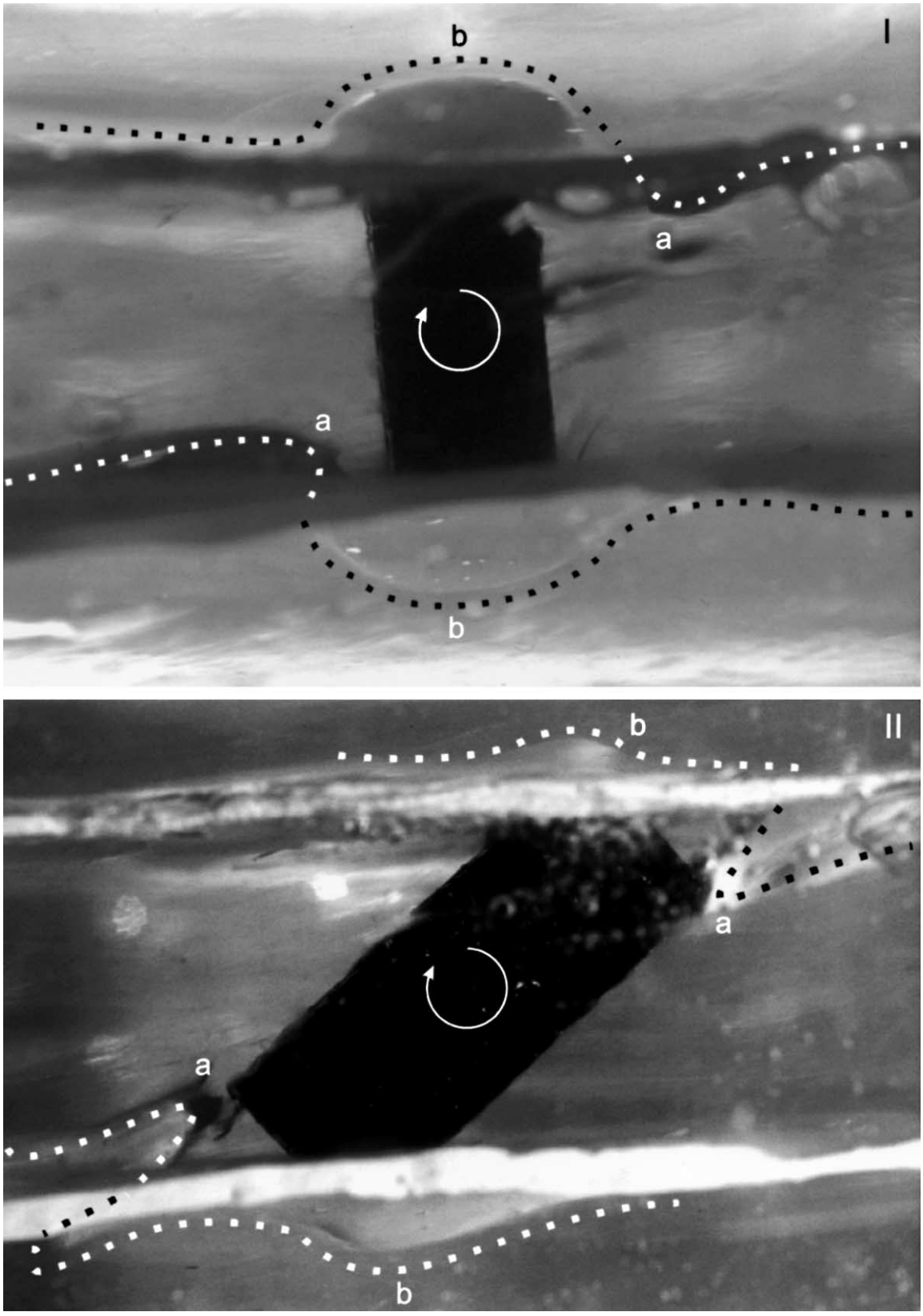

Fig. 6. Photos of *XZ* views of experiment 2 (Table 1) to illustrate sheath fold development by drag pull (a) and formation of transient deflections (b) by drag push and pull during top to the right shearing (for direct comparison with Fig. 1B).

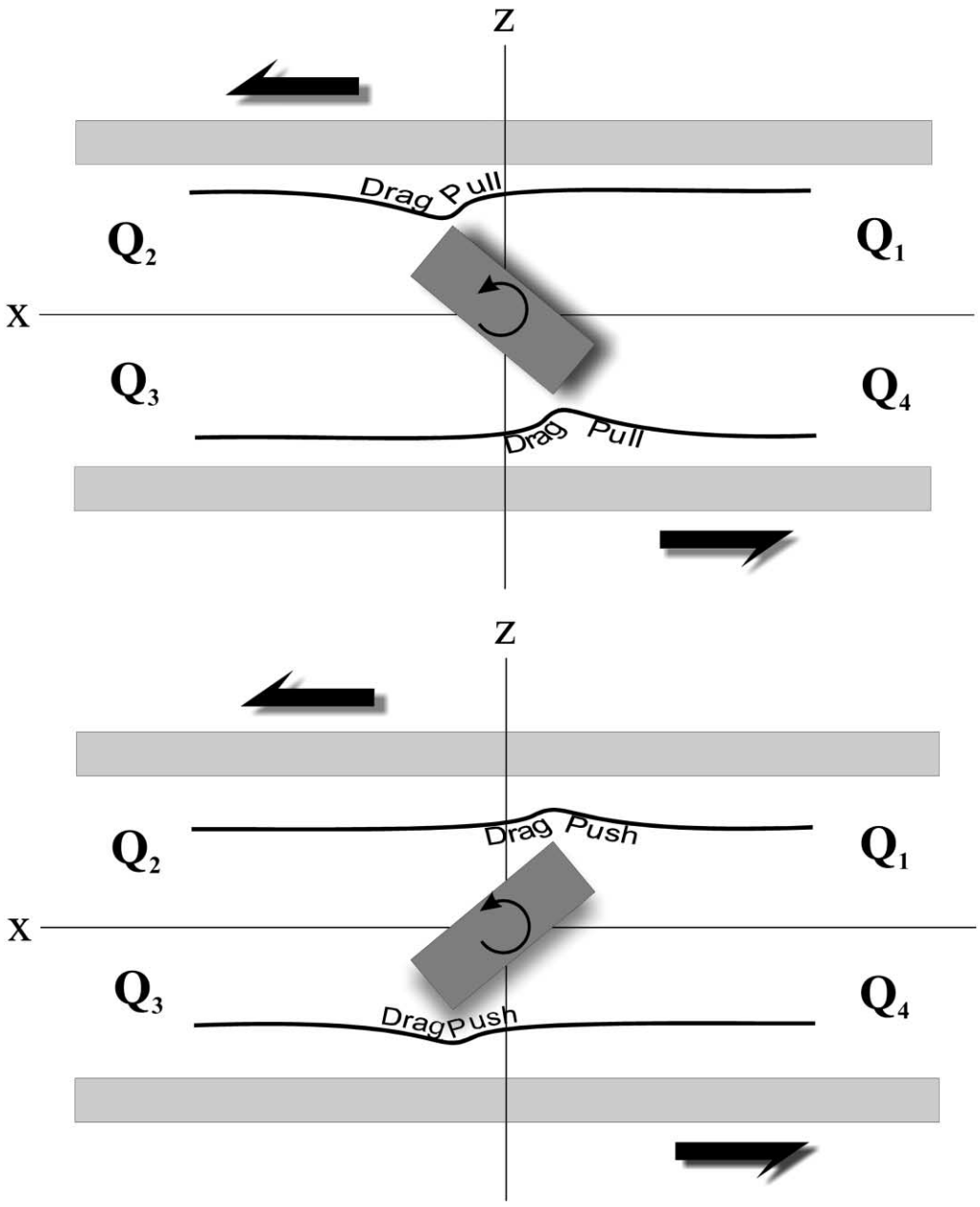

Fig. 7. Schematic diagram to show the quadrants (Q_1–Q_4) of dominant drag-pull and drag-push induced by rotation of the rigid inclusion.

4. Results and discussion

Table 1 summarises the results of all experiments.

4.1. First set of experiments: $d \approx 5$ mm

In the present set of experiments $R \approx 2.5$ and $E \approx 1.40$ (for $\phi_0 = 0°$) or $E \approx 0.80$ (for $\phi_0 = 90°$). The variables were the initial shape of the marker layer and ϕ_0 (Table 1, experiments 1–4).

4.1.1. Initial planar marker layer — results

When $\phi_0 = 0°$ the inclusion rotated synthetically and the passive marker layer remained planar (Table 1, experiment 1).

When $\phi_0 = 90°$ the inclusion rotated synthetically and two main features were observed as ϕ increased: (1) two non-cylindrical deflections formed in the marker layers towards the centre of the shear zone, known as inwards deflections (Table 1, experiment 2b and Fig. 6Ia); (2) two non-cylindrical deflections formed on the planar marker layers towards the shear zone walls. These are outwards deflections (Table 1, experiment 2b and Fig. 6Ib). After a rotation of 180° the outwards deflections vanished (transient non-cylindrical deflections), whereas the inwards deflections were enhanced to form sheath folds defining a monoclinic geometric pattern (Table 1, experiment 2c and Fig. 6II).

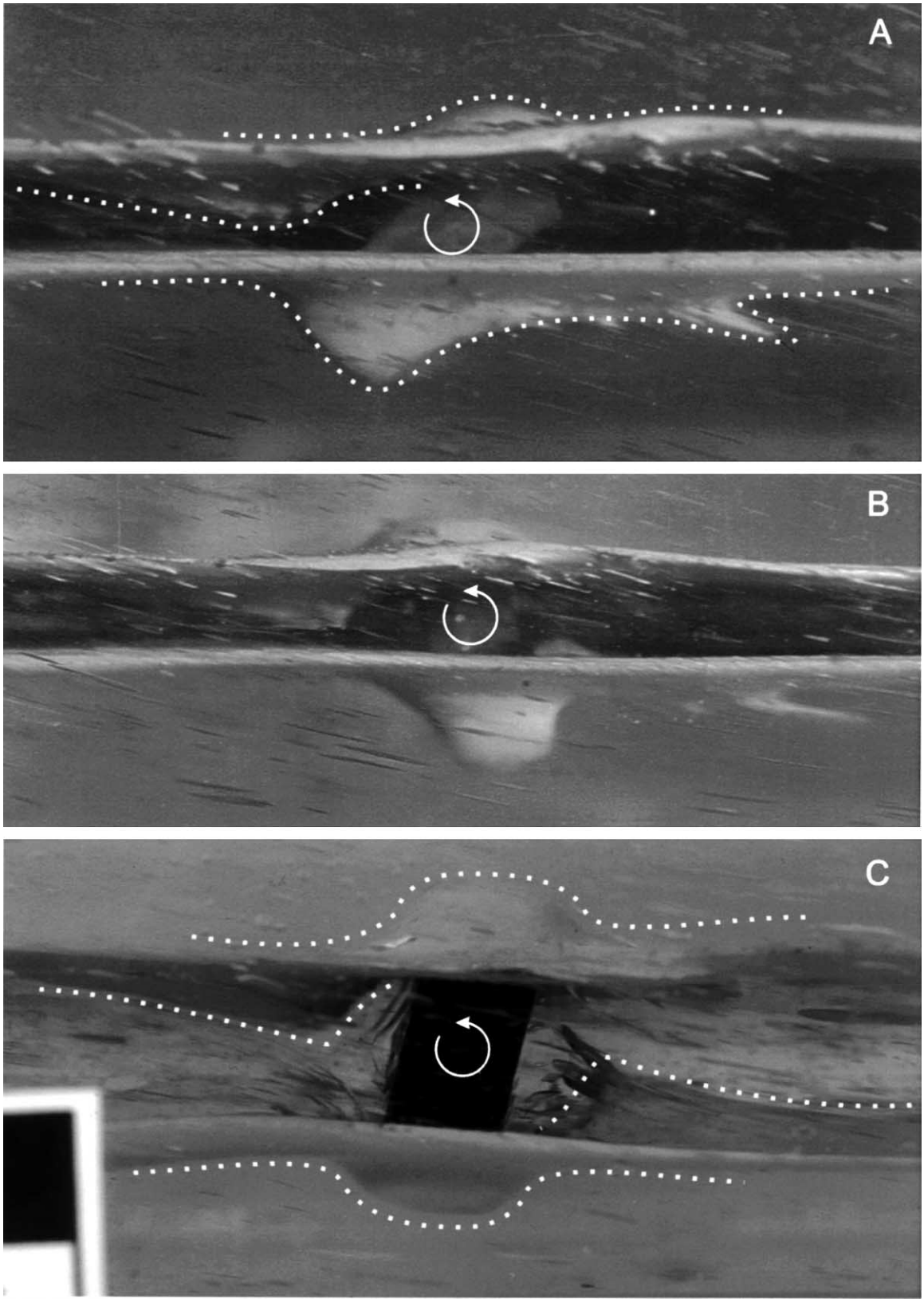

Fig. 8. Photos of *XZ* views of experiments 4 (A and B) and 6 (C) (cf. Table 1). Top to the left shearing. See text for explanation.

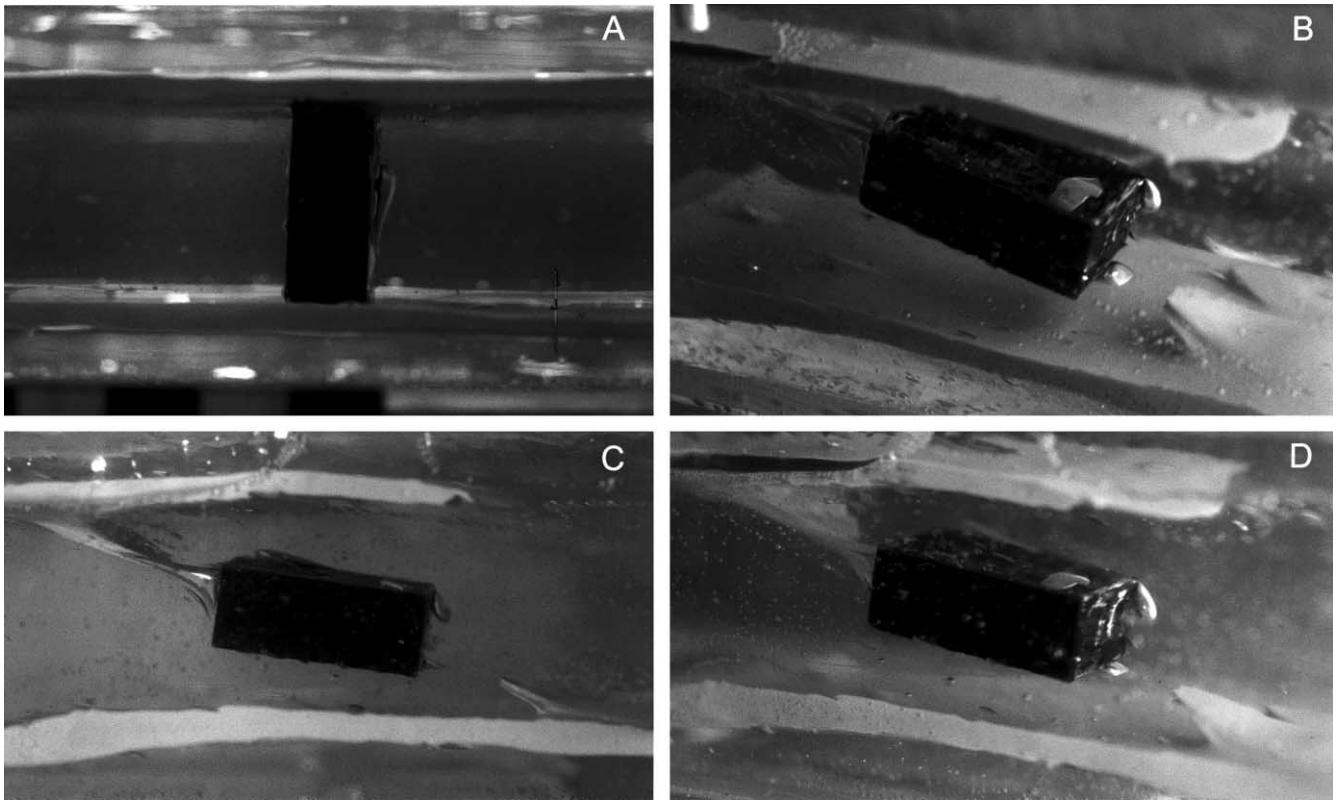

Fig. 9. Photos of *XZ* views of experiment 5 to illustrate sheath fold development by drag pull during top to the left shearing. (A) Initial stage. (B) Oblique view after 50° of anticlockwise rotation; the two sheath folds closer to the observer and to the tops of the particle were produced by rotation of the inclusion, but other minor sheath folds scattered on the surface of the marker layer resulted from shearing of trapped air bubbles in between layers. (C) Final stage. (D) Oblique view of final stage for a better visualisation of sheath fold shape.

4.1.2. Initial planar marker layer — discussion

When $\phi_0 = 0°$ and $E \approx 1.40$, the inclusion and the marker layers seemed to behave independently of each other: the inclusion rotated synthetically as theoretically predicted by Ghosh and Ramberg (1976) (Fig. 5), but the passive marker layer remained unstrained regardless of inclusion rotation. This result suggests that the flow close to the marker layer was laminar, in the sense that slip vectors did not change direction. Thus, for $E > 1.40$ the layers are unstrained by particle rotation in the conditions of the experiments.

When $\phi_0 = 90°$ and $E \approx 0.80$, D is smaller than the a value of the inclusion, in contrast with the above case of $\phi_0 = 0°$ and $E \approx 1.40$. Homogeneous simple shear is characterised by parallel slip vectors. However, when there is a rigid body immersed in a fluid subject to viscous simple shear flow, the flow pattern is perturbed in its vicinity and slip vectors are no longer parallel. Therefore, we have distinguished between quadrants in which the lines defined by slip vectors become depressed towards the rigid body or salient outwards from the rigid body (Fig. 7). In this last case we define drag by push, which takes place during the first 90° of synthetic rotation from $\phi_0 = 90°$ (Table 1, experiment 2b and Figs. 6Ib and 7), because the rigid inclusion indents and deflects the viscous PDMS towards the shear zone walls. In the former case we define drag by pull, which occurs between 90 and 180° of rotation of the particle (Table 1, experiment 2 and Figs. 6IIa and 7). In the conditions of $\phi_0 = 90°$ and $E \approx 0.80$, between 90 and 180° of rotation, the earlier-formed outwards deflections began to vanish because the drag effect was locally reversed (pulling instead of pushing — Fig. 6IIb). Conversely, in the sites where inwards deflections formed, drag by pull was constant and deflections grew into well-developed sheath to tubular folds (Table 1, experiment 2c and Fig. 6Ia and IIa).

Our experimental pattern of sheath folds is different from the ones obtained by Cobbold and Quinquis (1980, Fig. 1) and Marques and Cobbold (1995, Fig. 12). In these two works, sheath folds developed from non-cylindrical initial deflections on the layers surrounding the rigid inclusions and were outwards deflections (thus, sheath fold apexes pointed away from inclusions), whereas in the present study sheath folds developed from planar layers and inwards deflections (thus, the apexes pointed towards the inclusion).

Compared with our field example (Fig. 1B) there is a striking resemblance between the fold pattern around the upright standing boudin, and the intermediate stage of our experiment 2 of Table 1 (compare Fig. 1B with Fig. 6I and II). The development of the natural fold pattern could have resulted from clockwise rotation of the boudin and differential drag of the layers. Layers closer to the boudin are

dragged by pull to form sheath folds (Fig. 1Ba) and dragged by push to form deflections (Fig. 1Bb) that later could decrease or even vanish instead of evolving to sheath folds according to previously published models (Cobbold and Quinquis, 1980; Marques and Cobbold, 1995; Rosas et al., 2001). Layers progressively further from the boudin are gradually less affected by the rotation of the rigid body.

4.1.3. Initial deflected marker layer — results

Regardless of the ϕ_0 of the inclusion in these experiments, sheath folds developed from the original non-cylindrical deflections in the marker layers (Table 1, experiments 3 and 4 and Fig. 8A and B). The overall structure consists of two sheath folds around the inclusion, defining a monoclinic pattern from which shear sense can be determined (Table 1, Experiments 3c and 4c).

For final stages with $\gamma \approx 5$, ω was approximately equal to 28° and $x/y \approx 2$.

4.1.4. Initial deflected marker layer — discussion

The results of our experiments are similar to those of Cobbold and Quinquis (1980), Marques and Cobbold (1995) and Rosas et al. (2001).

4.2. Second set of experiments: $d \approx 2$ mm

In the present set of experiments $R \approx 2.5$ and $E \approx 1.16$ (when $\phi_0 = 0°$) or $E \approx 0.56$ (when $\phi_0 = 90°$). We used both planar and curved initial shapes of the marker layer and variable ϕ_0 (Table 1, experiments 5–8).

4.2.1. Initial planar marker layer — results

Regardless of the original orientation of the inclusion, drag sheath folds developed from the planar marker layers (Table 1, experiments 5 and 6 and Figs. 8C and 9A–D), defining a pattern similar to the one described above for experiment 2 of Table 1 (compare final results of experiments 2 and 5).

In the case of $\phi_0 = 90°$, besides the above mentioned drag sheath folds, other sheath folds developed from the deflections generated by the rotation of rigid inclusions (Table 1, experiment 6), similar to the ones described by Cobbold and Quinquis (1980), Marques and Cobbold (1995) and Rosas et al. (2001).

For final stages with $\gamma \approx 4$, drag sheath folds showed $\omega \approx 50°$ and $x/y \approx 2$ for $\phi_0 = 90°$, and ω was approximately equal to 48° and $x/y \approx 1$ when $\phi_0 = 0°$.

4.2.2. Initial planar marker layer — discussion

Similarly to the first set of experiments with initial planar marker layers ($\phi_0 = 90°$), we interpret these results as a consequence of drag on the marker layers close to the inclusion. In the present case ($\phi_0 = 0°$), however, $E \approx 1.16$, which means that D was greater than a and hence only drag by pull could occur during the $\approx 90°$ rotation of the inclusion (see variation of drag by push and pull in Fig. 7). Drag by push would be possible only if $E < 1.4$ and $\phi_0 = 90°$, or a rotation of at least 180° of the inclusion starting with $\phi_0 = 0°$ (see distribution of push and pull in quadrants of Fig. 7).

In experiment 6, E was smaller than in experiment 2 ($E = 0.56$ and 0.80, respectively), which resulted in two main differences: (1) after 90° of inclusion rotation, the inwards non-cylindrical deflections were more developed in experiment 6 than in experiment 2, showing that the drag effect (flow perturbation) increased towards the inclusion (lower value of E); and (2) the two outwards non-cylindrical deflections in experiment 6 did not vanish as in experiment 2, and originated sheath folds instead. This shows that for a lower value of E, indentation of the marker layers by the rigid particle is greater and subsequent drag by pull was not enough to destroy the earlier formed outwards deflection.

In experiments 1 and 5 of Table 1, E was always greater than 1 ($E \approx 1.40$ and 1.16), but d was smaller in experiment 5. Hence, in experiment 1, the slip vectors close to the marker layers must have kept direction constant, whereas in experiment 5, slip vectors must have changed direction as a result of particle rotation and drag by pull occurred generating sheath folds.

4.2.3. Initial deflected marker layers — results and discussion

In the experiments with both $\phi_0 = 90°$ and $\phi_0 = 0°$, the end results (Table 1, experiments 7 and 8) showed a combined effect of drag by push and pull (discussed above), and by mechanisms already described by Cobbold and Quinquis (1980), Marques and Cobbold (1995) and Rosas et al. (2001).

For final stages with $\gamma \approx 5$, ω was approximately equal to 29° and $x/y \approx 4$ for $\phi_0 = 90°$, and ω was approximately equal to 29° and $x/y \approx 2$ for $\phi_0 = 0°$.

5. Conclusions

Sheath folds can develop from planar surfaces around rigid inclusions, in bulk simple shear without concomitant boudinage processes. Such folds develop by drag pull and depend on the distance of the marker layers from the rigid inclusion.

Some outwards non-cylindrical deflections are transient and, thus, do not produce sheath folds. Transient deflections depend on the ratio E between the distance between marker layers and the greater principal dimension of the boudin.

The monoclinic symmetry of drag sheath fold patterns associated with rotating rigid inclusions indicate non-coaxial flow and can be used as a shear sense criterion.

Acknowledgements

The experiments were performed in the Experimental

Tectonics Laboratory of LATTEX, a research unit funded by PLURIANUAL, Project 125/N/92. Field work of F. Marques was supported by the same project. F. Rosas acknowledges a Ph.D. scholarship (PRAXIS XXI/BD/9220/96) of FCT. We thank L. Skjernaa and an anonymous reviewer for their careful and constructive reviews which helped improve the manuscript.

References

Cobbold, P.R., Quinquis, H., 1980. Development of sheath folds in shear regimes. Journal of Structural Geology 2, 119–126.

Ghosh, S.K., Ramberg, H., 1976. Reorientation of inclusions by combination of pure shear and simple shear. Tectonophysics 34, 1–70.

Marques, F.G., Cobbold, P.R., 1995. Development of highly non-cylindrical folds around rigid ellipsoidal inclusions in bulk simple shear regimes: natural examples and experimental modelling. Journal of Structural Geology 17, 589–602.

Ramberg, H., 1959. Evolution of ptygmatic folding. Norsk Geologisk Tidsskrift 39, 99–161.

Rosas, F., Marques, F.O., Coelho, S., Fonseca, P., 2001. Sheath fold development in bulk simple shear: analogue modelling of natural examples from the Southern Iberian Variscan Fold Belt. In: Koyi, H.A., Mancktelow, N. (Eds.), Tectonic Modeling: A Volume in Honor of Hans Ramberg. Geological Society of America Memoir 193, pp. 103–115.

Skjernaa, L., 1989. Tubular folds and sheath folds: definitions and conceptual models for their development, with examples from the Grapesvare area, northern Sweden. Journal of Structural Geology 11, 689–703.

Talbot, C.J., 1999. Can field data constrain rock viscosities? Journal of Structural Geology 21, 949–957.

Treagus, S.H., 1999. Are viscosity ratios of rocks measurable from cleavage refractions? Journal of Structural Geology 21, 895–901.

Van Den Driessche, J., Brun, J.-P., 1987. Rolling structures at large shear strain. Journal of Structural Geology 9, 691–704.

Weijermars, R., 1986. Flow behaviour and physical chemistry of bouncing putties and related polymers in view of tectonic laboratory applications. Tectonophysics 124, 325–358.